We are IntechOpen, the world's leading publisher of Open Access books Built by scientists, for scientists

6,900
Open access books available

185,000
International authors and editors

200M
Downloads

Our authors are among the

154
Countries delivered to

TOP 1%
most cited scientists

12.2%
Contributors from top 500 universities



WEB OF SCIENCE™

Selection of our books indexed in the Book Citation Index in Web of Science™ Core Collection (BKCI)

Interested in publishing with us?
Contact book.department@intechopen.com

Numbers displayed above are based on latest data collected.
For more information visit www.intechopen.com



4

Characterization Parameters of (InGaN/InGaN) and (InGaN/GaN) Quantum Well Laser Diode

Sabah M. Thahab
College of Engineering, University of Kufa, Iraq

1. Introduction

Laser characterization can facilitate improvement in laser design by allowing optical component scientists to compare different laser designs and to confirm the validity of their theories behind their designs. Various desired characteristics of a laser are discussed. All of the following characteristics will be taken into consideration seriously during laser design. The most important operating parameters in InGaN LDs are the internal quantum efficiency (η_i) , the internal loss α_i and the transparency current density J0 as these are the key parameters which control the operating characteristics of LDs. The characteristic temperature is also a very important parameter from the viewpoint of the practical application of these lasers. Well-number effect on the characteristics temperature will also be investigated through the simulation software. Experimental and theoretical work done by Domen et al. (1998) concluded that the InGaN laser diode quantum efficiency improves when the number of wells is decreased. Our work supports prior research results.

2. Construction of a blue laser diode structure

III-nitride semiconductor materials have received much attention in the past few years since they have important applications in light-emitting diodes (LEDs) and short wavelength laser diodes (LDs), due mainly to their relatively wide band gap and high emission efficiency. Especially after the development of the InGaN blue LDs that can be continuously operated for more than 10 000 h, and the InGaN LED that can emit light in the red spectral range, III-nitride semiconductor materials have become the most attractive materials among III-V and II-VI semiconductors (Jiang and Lin, 2001).

However, for commercial applications, LD and LED markets in the red and yellow spectral range are still dominated by the AlGaInP semiconductor materials. This is due to the fact that InGaN devices are usually more expensive, and many aspects of the physics related to III-nitride semiconductor materials have not been well developed. When a LD is under operation, current overflow will cause a decrease in emission efficiency and an increase in the device temperature, which in turn results in the deterioration of the operation lifetime. There are many factors that might cause the current overflow.

The III-nitride LDs structure is shown in Fig. 1 the first possible cause of the overflow is the relatively small band-offset ratio between the conduction band and the valence band (Kuo et al., 2004). Under these circumstances, the potential difference between the quantum well and the barrier in the conduction band is relatively small and, hence, the electrons can easily overflow to the p side. The second factor that might cause the electronic current overflow is the high threshold currents of III-nitride LDs. Due to the lack of a lattice-matched substrate; the InGaN LDs usually have a high density of crystal defects. Moreover, high-quality p-type layers and flat reflecting mirrors are usually difficult to obtain. These problems ultimately lead to a high threshold current of the InGaN LD, which in turn increases the temperature of the LD and the possibility of current overflow (Nakamura and Fasol, 1997).

The third possible cause of electronic current overflow is the difficulty with which the holes enter the active region, due mainly to the high effective mass of the holes and the high band-offset in the valence band. Since the holes cannot easily enter the active region, more current is required to activate the laser action, thus increasing the possibility of electronic current overflow.

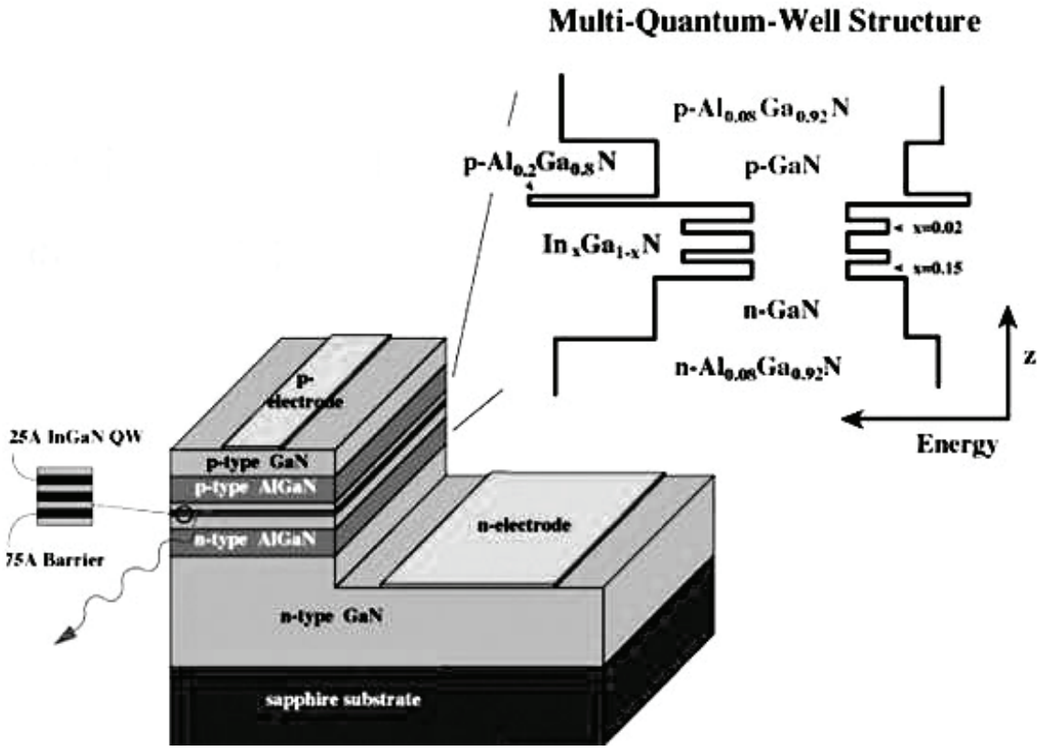


Fig. 1. The structure of InGaN multi quantum wells laser diode. (Ponce 1997)

On the other hand, Nakamura et al. studied the laser performance of several LDs with an emission wavelength of 390–420 nm as a function of the number of InGaN well layers Fig. 1. They found that the lowest threshold current density was obtained when the number of InGaN well layers was two. In addition the successes to handle the carrier overflow by using AlGaN as blocking layer as shown in Fig. 2. However, in another study, they observed that in LDs with emission wavelengths longer than 435 nm, when the number of InGaN well

layers varied from one to three, the threshold current density was lowest at one, and increased with the number of InGaN well layers. This phenomenon was attributed to the dissociation of the high indium content of the InGaN well layer at a high growth temperature of 750 °C due to a high InGaN dissociation pressure

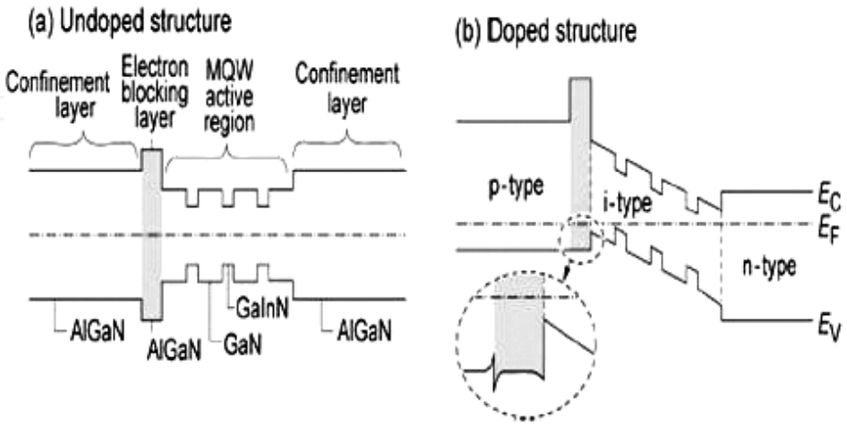


Fig. 2. The AlGaN current –blocking layer in an AlGaN/GaN/GaInN multi quantum wells. (a) Band diagram without doping. (b) Band diagram with doping. The Al content in the electron – blocking layer is higher than in the p-type confinement layer.

3. InGaN laser diode simulation procedure

The 2-D laser diode device simulations are performed using ISE-TCAD package. A conventional simulation flow would include three steps:

1. Drawing cross-sectional view of device and generating mesh in MDraw.
2. Performing 2-D device simulation using DESSIS.
3. Plotting data curves of interest and extracting parameters using INSPECT.

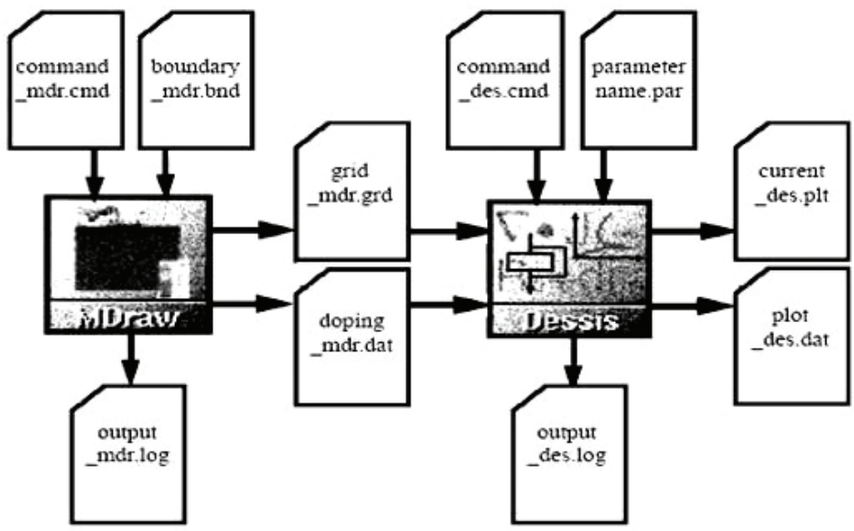


Fig. 3. Typical design flow with DESSIS device simulation. (Manual of Integrated System Engineering (ISE TCAD) AG, Switzerland)

DESSIS is used to simulate the electrical and optical characteristics of the device. Such a seamless flow through ISE TCAD tools, with the associated file types, is represented in Fig. 3. Finally, Tecplot-ISE is used to visualize the output from the simulation in 2D, and INSPECT™ is used to plot the electrical and optical characteristics.

3.1 The fundamental set of equations used in a laser simulation

Simulating a laser diode is one of the most complex problems in device simulation. The fundamental sets of equations used in a laser simulation are:

1. Poisson equation
2. Carrier continuity equations
3. Lattice temperature equation and hydrodynamic equations
4. Quantum well scattering equations (for QW carrier capture)
5. Quantum well gain calculations (Schrödinger equation)
6. Photon rate equation
7. Helmholtz equation

3.2 Coupling between optics and electronics problems

The complexity of the laser problem is apparent from the relational chart shown in Fig. 4. The key quantities exchanged between different equations are placed alongside the directional flows between the equation blocks. The optical problem must be separated from the electrical problem.

The optical problem solves the Helmholtz equation and feeds the mode and photon lifetimes back to the set of active vertices. As a result, the coupling between the optics and electronics becomes nonlocal, and this leads to convergence problems if the Newton method is used to couple these two problems. Therefore, a Gummel iteration method (instead of a coupled Newton iteration) is required to couple the electrical and optical problems self-consistently. The solution of the electrical problem provides the required refractive index changes and absorption to the optical solver, which solves for the modes. In the case of the Fabry–Perot edge-emitting laser, the wavelength is computed from the peak of the gain curve and fed into the optical problem.

Poisson equation

$$\nabla.(\varepsilon\nabla\Phi) = q(n - p - N_D^{+} + N_A^{-}) \tag{1}$$

Electron continuity equation

$$\frac{\partial n}{\partial t} - \nabla.J_n = q(G_n - R_n) \tag{2}$$

Hole continuity equation

$$\frac{\partial p}{\partial t} + \nabla.J_p = q(G_p - R_p) \tag{3}$$

$$J_n = q(-\mu_n n \nabla \Phi + D_n \nabla n) \tag{4}$$

$$J_p = q(-\mu_p p \nabla \Phi - D_p \nabla p) \tag{5}$$

In vertical cavity surface emitting laser diodes (VCSELs) and distributed Bragg reflector (DBR) lasers, the wavelength is computed inside the optical resonance problem and is an input to the electrical problem instead. The gain calculations involve the solution of the Schrödinger equation for the subband energy levels and wavefunctions. These quantities are used with the active-region carrier statistics to compute the optical matrix element in the material gain. The photon rate equation takes the material gain and mode information to compute the modal gain and, subsequently, the stimulated and spontaneous recombination rates. These optical recombinations increase the photon population but reduce the carrier population. Therefore, these recombination rates must be added to the carrier continuity equations to ensure the conservation of particles.

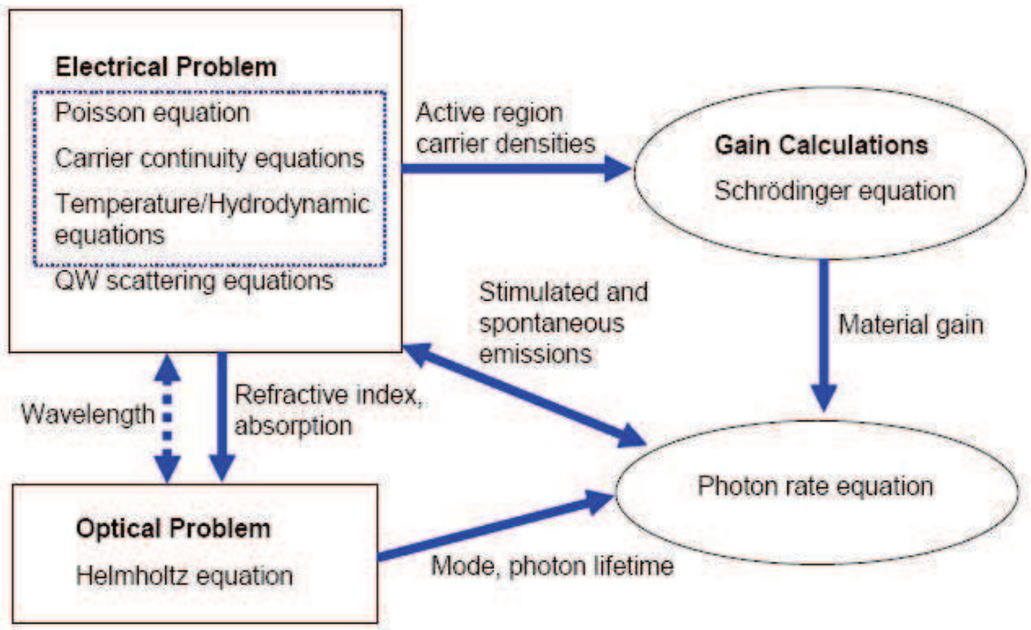


Fig. 4. The coupling between optics and electronics problems. (Manual Integrated System Engineering (ISE TCAD) AG, Switzerland)

From its bandgap dependence in other materials, a very small Auger parameter of $c = 10^{-34}$ cm6 s^{-1} is estimated for GaN. Thus, even with large carrier densities, Auger recombination in nitride materials is negligible. A wide spectrum of bandgap bowing parameters has been obtained for ternary nitride alloys due to differences in growth and measurement conditions. For layers with low mole fraction of the alloy element (x<0.2), we employ the following room temperature relations for the direct bandgap (Stringfellow and Craford, 1997; Nakamura and Fasol, 1997).

$$E_{g In_x Ga_{1-x} N} = x E_{g InN} + (1-x) E_{g GaN} - 1.43x(1-x) \tag{6}$$

$$E_{g\,Al_xGa_{1-x}N} = xE_{g\,AlN} + (1-x)E_{gGaN} - 1.3x(1-x) \tag{7}$$

Where Eg,InN, Eg,GaN and Eg,AlN are the bandgap energies of InN, GaN and AlN at room temperature ,respectively. The bandgap energies of InN, GaN and AlN used in our simulation are 0.77, 3.42 and 6.2 eV (Fritsch et al., 2003), respectively. A band offset ratio of $\Delta E_C / \Delta E_V = 0.7 / 0.3$ is assumed for InGaN/GaN as well as for AlGaN/GaN, which corresponds to an average of reported values for each case. In our strained InGaN quantum wells, binary effective mass parameters, lattice constants and elastic constants are determined from the linear interpolations to obtain InGaN values. GaN values are used for the deformation potentials (Fritsch et al., 2003).

$$m_{eIn_xGa_{1-x}N} = m_{eGaN} + x(m_{eInN} - m_{eGaN}) \tag{8}$$

$$m_{hhIn_xGa_{1-x}N} = m_{hhGaN} + x(m_{hhInN} - m_{hhGaN}) \tag{9}$$

$$m_{lhIn_xGa_{1-x}N} = m_{lhGaN} + x(m_{lhInN} - m_{lhGaN}) \tag{10}$$

where $m_{eInxGa1-xN}$ is the effective mass of electrons in $In_xGa_{1-x}N$ material. $m_{hhInxGa1-xN}$ and $m_{lhInxGa1-xN}$ are the effective masses of heavy holes and light holes in $In_xGa_{1-x}N$, respectively m_{eInN} for InN is 0.1 m_0 and m_{eGaN} for GaN is 0.20m_0. While m_{hhInN} and m_{lhInN} for InN are 1.44m_0 and 0.157m_0 , respectively, and for GaN m_{hhGaN} and m_{lhGaN} are 1.595m0 , 0,261m0 respectively, and m_0 is the electron mass in free space (Kuo et al., 2004) .The optical gain mechanism in InGaN quantum wells of real lasers is still not fully understood. It may be strongly affected by a non-uniform indium distribution. Internal polarization fields tend to separate quantum confined electrons and holes, thereby reducing optical gain and spontaneous emission. However, screening by electrons and holes is expected to suppress QW polarisation fields at high current operation. The high carrier density is also assumed to eliminate exciton effects, despite the large exciton binding energy in nitrides. On the other hand, many-body models predict significant gain enhancement at high carrier densities. Considering all the uncertainties in calculating the gain of our assumed rectangular quantum wells, we start with a simple free carrier gain model, including a Lorentzian broadening function with 0.1 ps scattering time.

Optical reflection and waveguiding mainly depends on the refractive index profile inside the device. For photon energies close to the bandgap, the refractive index is a strong function of wavelength. For the design of optical waveguides, the compositional change of the refractive index is often more important than its absolute value. Reliable refractive index measurements on $In_xGa_{1-x}N$ are currently not available so that a linear interpolation of binary parameters is chosen in this study. In addition, we employ the refractive index relations given in Eqs.(11) and (12), respectively (Sink, 2000).

Spontaneous polarization as well as strain-induced polarization in nitride compounds results in polarization charges at heterointerfaces and built-in polarization fields. We calculate these charges by linear interpolation of binary material parameters. Full consideration of the calculated polarization charges results in a strong deformation of the QW potential by the built-in QW polarization field.

$$n(In_xGa_{1-x}N) = 2.5067 + 0.91x \tag{11}$$

$$n(Al_xGa_{1-x}N) = 2.5067 - 0.43x \tag{12}$$

4. InGaN laser diode simulation results and discussion

A schematic diagram of the laser diode structure is shown in Fig. 5.. n-type GaN layer that is 3μm in thickness is assumed to grow first then followed by 0.4μm n-type $Al_{0.07}Ga_{0.93}N$ cladding layer, followed by a 0.1μm n-type GaN guiding layer. The active region of the preliminary laser diode structure under study consists of a 3 nm $In_{0.13}Ga_{0.87}N$ well that is sandwiched between 5 nm $In_{0.01}Ga_{0.99}N$ barriers. 0.02 μm p-$Al_{0.15}Ga_{0.85}N$ stopper layer is assumed to be grown on the top of active region, followed by 0.1 μm p-type GaN guiding layer then 0.4 μm p-$Al_{0.07}Ga_{0.93}N$ cladding layer and 0.1 μm p-GaN contact layer. The doping concentration of n-type and p-type are 5×10^{17} cm^{-3} and 5×10^{18} cm^{-3}, respectively. The active region length is 800 μm and the reflectivity of the two ends (left and right) facets assumed as Fabry –Perot cavity waveguide with R= 0.3 respectively.

For the preliminary LD structure under study, the energy band diagram, and electrostatic potential of the double quantum wells (DQWs) InGaN LD are shown in Fig. 6. The right side of the diagram is the n-side and the left side is the p-side of the laser diode. The horizontal axis is the distance along the crystal growth direction. The optical material gain inside the quantum wells is shown in Fig. 7.

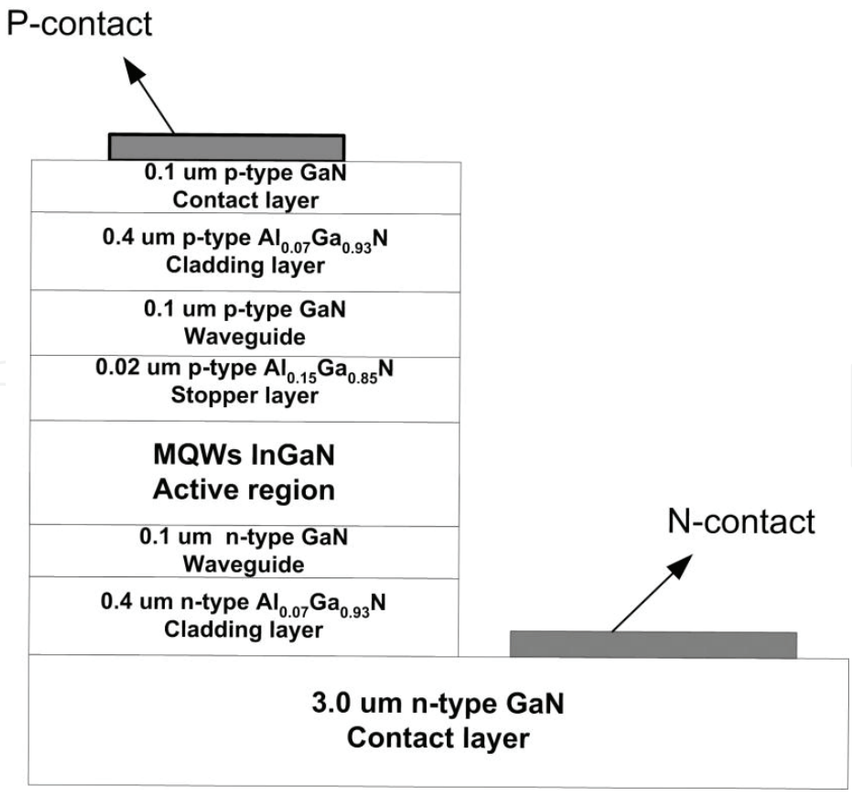


Fig. 5. Schematic diagram of the preliminary InGaN MQWs LD.

The quantum well in the left side (p-side) has a higher optical material gain due to the use of an AlGaN blocking layer in the p-side of which the electrons tend to accumulate in the left quantum well. Since holes have difficulty moving from the left quantum well to the right quantum well due to the relatively large effective mass, low mobility, and high band offset in the valence band, more holes are expected in the left quantum well.

Since the left quantum well possesses more electrons and holes as compared with the right quantum well, it has higher population inversion and hence higher stimulated recombination rate. The carriers (hole, electron) distribution inside the quantum wells determines the optical performance of the laser diode.

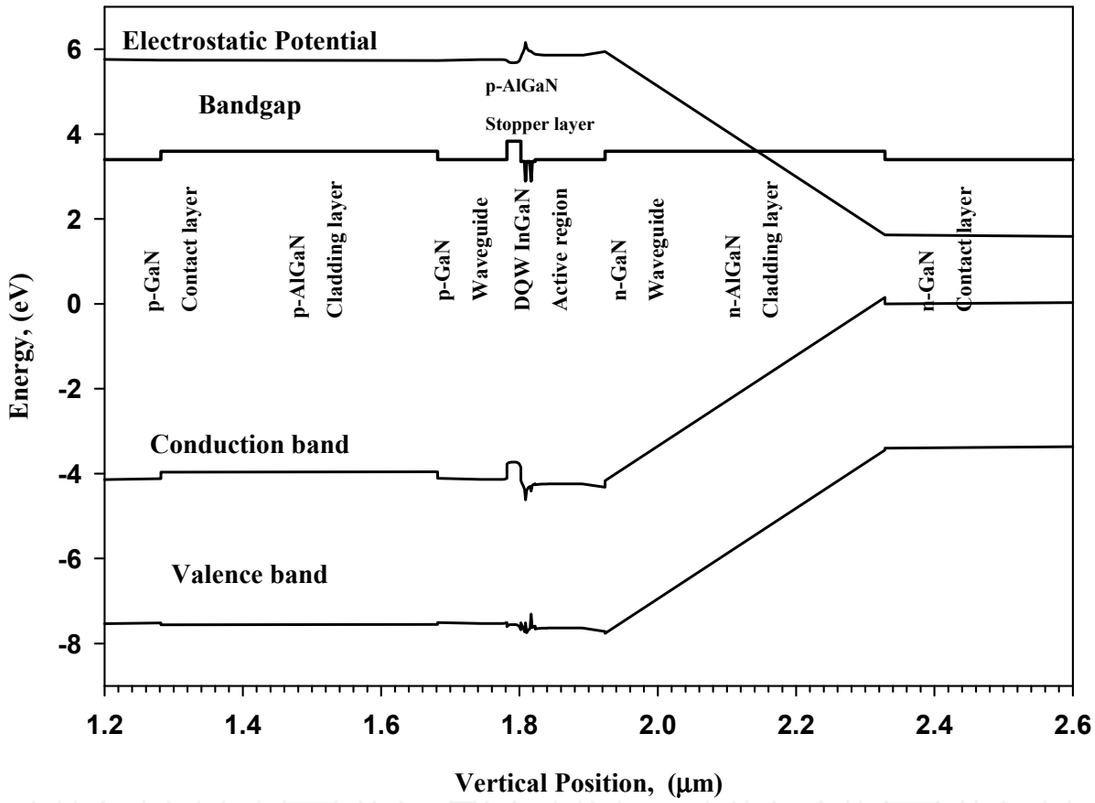


Fig. 6. Energy band diagram of the double quantum wells InGaN LD together with electrostatic potential profile.

From Fig. 8 it can be observed that the carrier distributions are inhomogeneous and are increasing towards the p-side. When the laser oscillation takes place, the hole injection becomes inhomogeneous among wells. This is ascribed to the poor hole injection due to the low mobility and thermal velocity of the hole. Thus the hole density becomes higher on the p-side and the electrons are attracted to the p-side. Optical reflection and waveguiding mainly depend on the refractive index profile inside the device. The laser threshold current, slope efficiency, output power and DQE at various well numbers are shown in Fig. 9. We observed maximum output power and lowest threshold current when the well number is two.

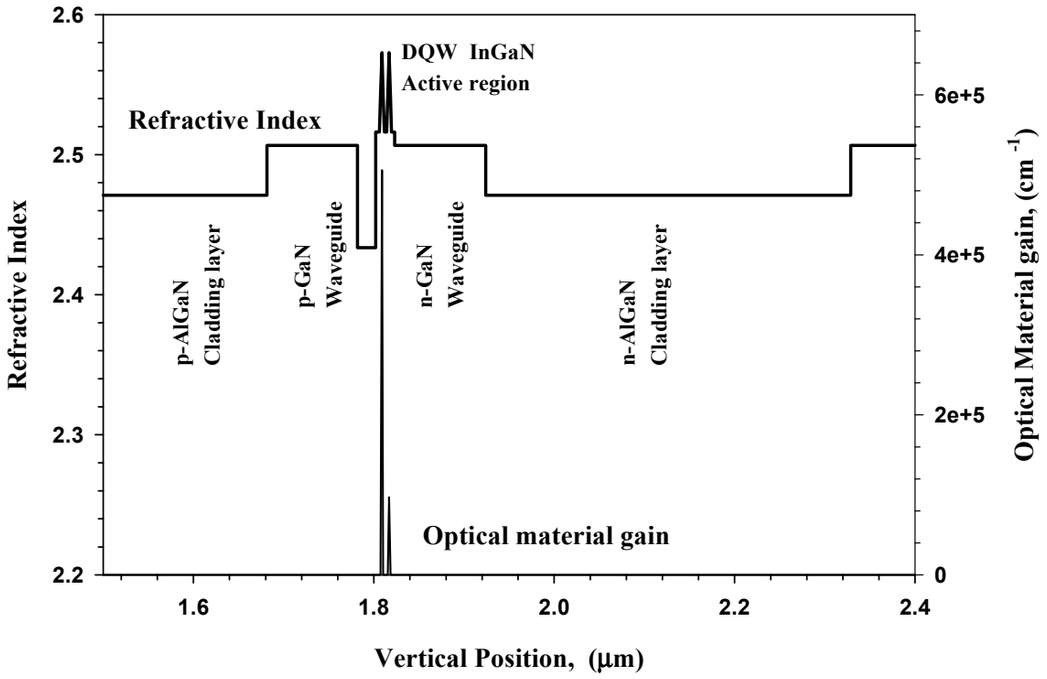


Fig. 7. Optical material gain in the InGaN double quantum wells LD.

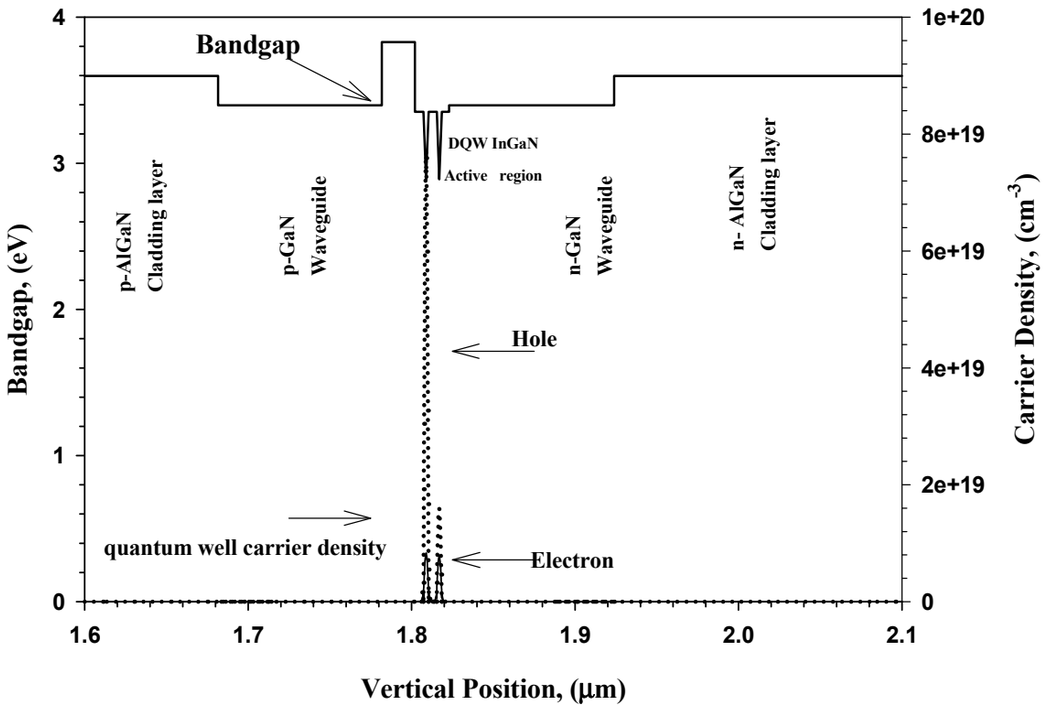


Fig. 8. Carriers density distribution profiles in the double quantum wells of InGaN LD.

These results are in agreement with the experimental results observed previously by Nakamura et al. (Nakamura et al., 1998a; Nakamura et al., 2000) in which they studied the laser performance of several laser diodes with an emission wavelength of 390-450 nm as a function of the number of InGaN well layers and found that the lowest threshold current was obtained when the number of InGaN well layers was two.Moreover, in another work they observed that when the number of InGaN well layers of the laser diodes with emission wavelengths longer than 435 nm was varied from one to three, the lowest threshold current was obtained when the number of well layers was one and the threshold current increased when the number of InGaN well layers was increased. This phenomenon was attributed to the dissociation of the high indium content InGaN well layer at a high growth temperature of 750 0C due to a high InGaN dissociation pressure. It was observed the deterioration in laser performance with increased quantum wells number in our simulation results, and attributed it to the non-uniform carrier distribution in the quantum wells. Nakamura assumption (the indium dissociation) did not take in our simulation process. The specified wavelength was selected to be the peak of the stimulated emission.

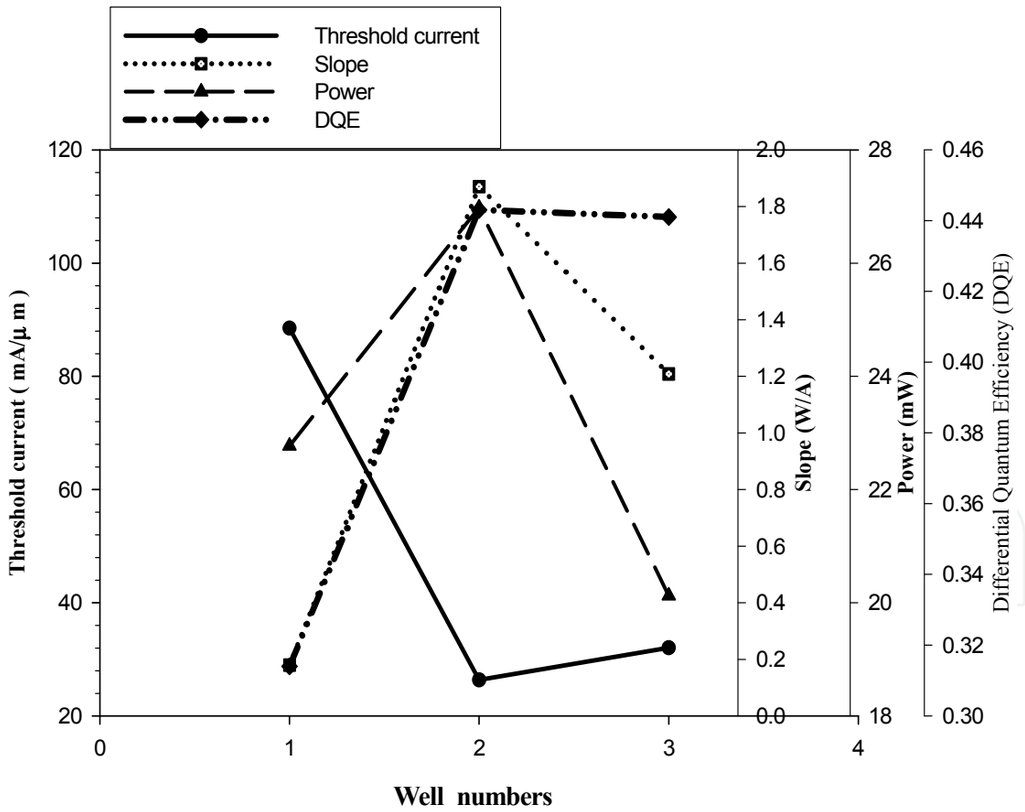


Fig. 9. Laser output power, slope efficiency, threshold current and differential quantum efficiency (DQE) as a function of well number of the MQWs InGaN LD.

The presence of the built-in electric field modifies the electronic states in QWs and lowers the optical gain of the active region of the laser as shown in Fig.10. The electrons and holes are, indeed, spatially separated by the polarization filed, but the free carrier induced field is opposite to the polarization field. The two fields tend to cancel each other out for higher sheet densities, thus re-establishing the conditions for the electron hole recombination emission. The wavelength of the light emitted from LD QW depends not only on the band gap, but also on the large internal electric field due to piezoelectric (PZ) and spontaneous polarization.

The PZ field arises from the strain due to the lattice mismatch between the InGaN well and the GaN barriers and causes redshift in the optical transition energy. The presence of the internal field in InGaN quantum wells causes separation of the electron and hole wave functions thus reducing the wave function overlap integral. As the carrier density in the quantum well increases, screening of the internal field occurs, hence a blue shift (418.5-415 nm) of the emission is observed in our laser diode.

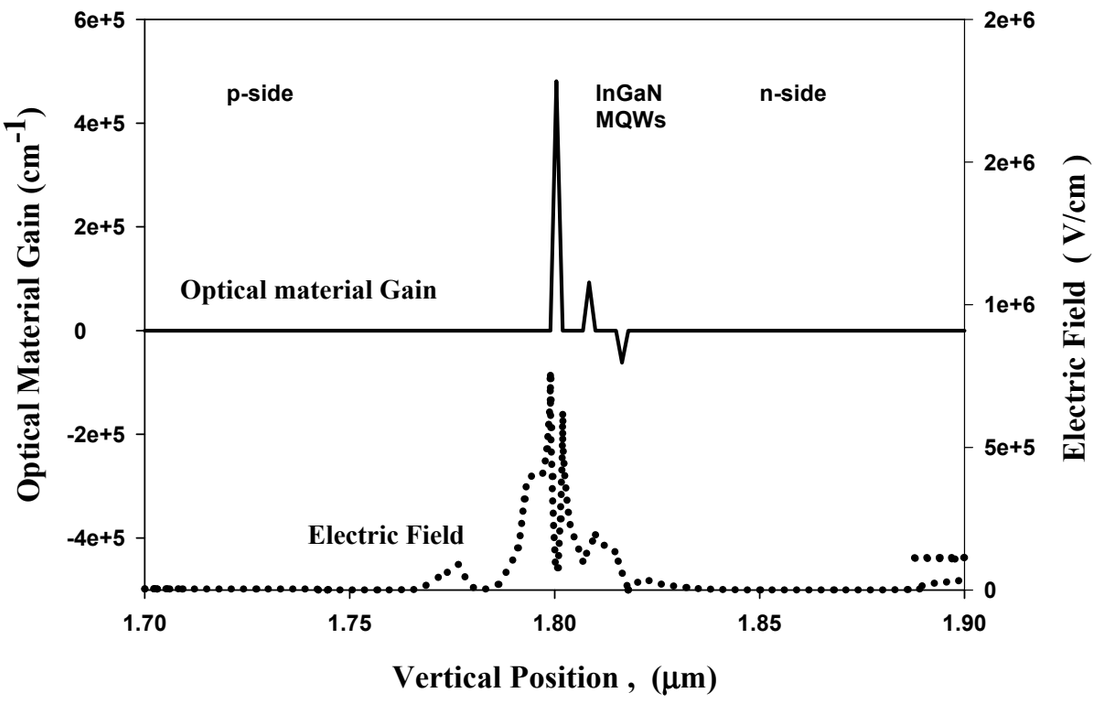


Fig. 10. Optical material gain in the InGaN TQWs LD together with internal electric field.

5. Test and characterization of InGaN/InGaN laser diode

5.1 The internal quantum efficiency η_i and internal loss α_i

The internal quantum efficiency (η_i) is determined from the vertical axis intercept point $(1/\eta_i)$ of the inverse external differential quantum efficiency (DQE) versus cavity length

dependence linear fit line. Internal loss α_i is equal to the slope of the line multiplied by the $\eta_i \ln(1/R)$ parameter, where L is the laser cavity length in units of cm and R is the reflectivity of the mirror facets of the laser. Fig.11 shows the calculation method for both parameters (η_i and α_i) with respect to inverse value of DQE as a function of the cavity length. We obtained values of 95% and 9.38 cm-1 for the internal quantum efficiency (η_i) and internal loss (α_i) respectively in the case of DQWs laser diode. These internal quantum efficiency (η_i) and the internal loss α_i values are a direct indication of the efficiency of our DQWs InGaN laser diode. It can be seen that the value of the external differential quantum efficiency (η_d) is smaller than internal quantum efficiency, and this difference is related to the different internal loss mechanism in the laser diode device.

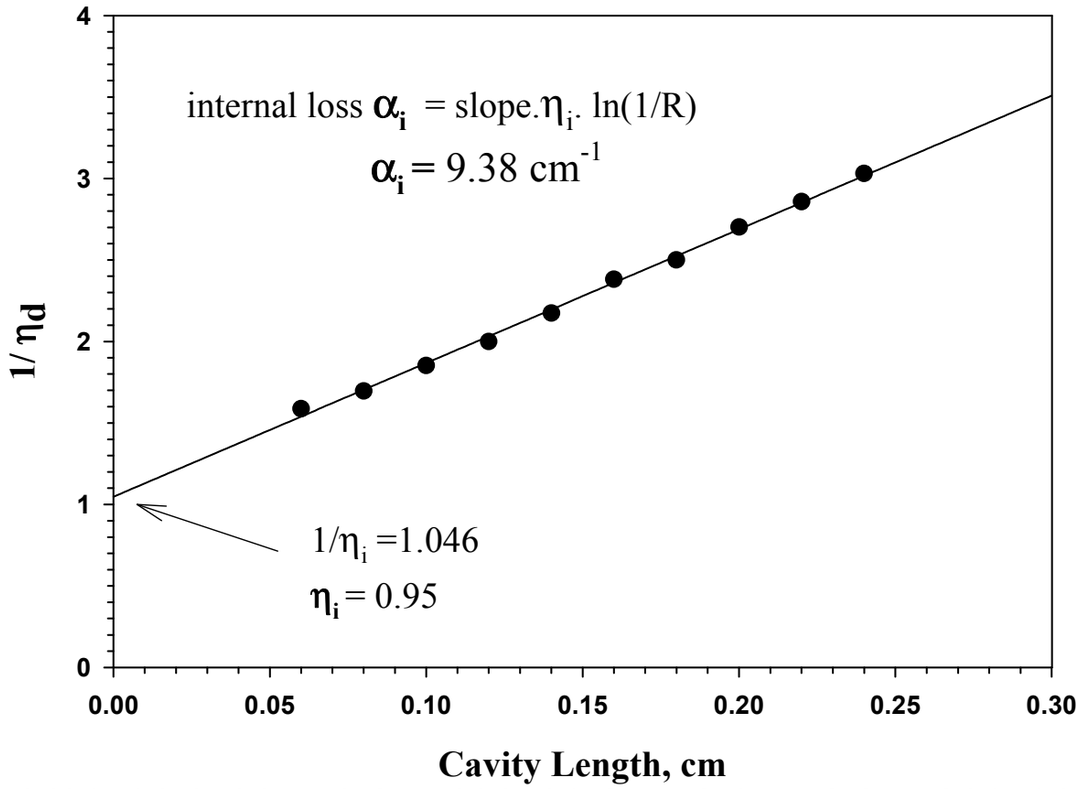


Fig. 11. Inverse of the external quantum efficiency as a function of cavity length of DQWs InGaN/ InGaN barrier LD .

5.2 Transparency threshold current density

The transparency threshold current density is denoted by the symbol J_0. Threshold current density depends upon the cavity length of the laser diode. The laser diode current that provides just sufficient injection to lead to stimulated emission just balancing absorption is called transparency current. Since there is no net photon absorption, the medium is transparent. Above transparency current there is optical gain in the medium

though the optical output is not yet a continuous wave coherent radiation. Lasing oscillation occur only when the optical gain in the medium can overcome the photon losses from the cavity that is when the optical gain reaches the threshold gain g_{th} and this occurs at the threshold current density. In order to obtain J_0 value we plot the curve of threshold current density versus the inverse cavity length as shown in Fig..12. The intercept of the linear fit line of the data plotted in this curve with the vertical axis provides us with the transparency threshold current density value. Value of 397 A/cm² is obtained for our DQWs laser diodes structure.

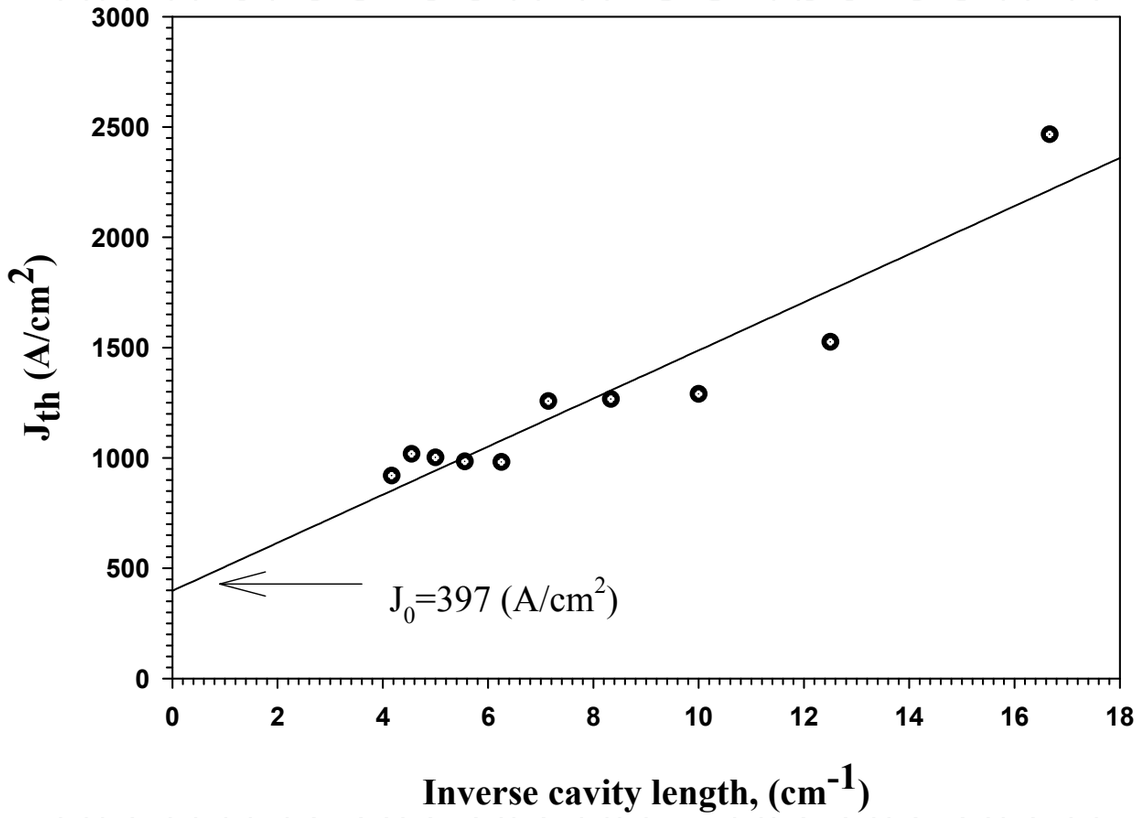


Fig. 12. The threshold current density as a function of inverse cavity length of DQWs InGaN/ InGaN barrier LD.

5.3 Characteristic temperature T_0

Higher values of characteristic temperature T_0 imply that the threshold current density and the external differential quantum efficiency of the device increase less rapidly with increasing temperatures. This translates into the laser being more thermally stable. The T_0 is determined by plotting the threshold current density (J_{th}) versus the laser device temperature on a logarithmic scale and then measuring the slope of the linear fit line as shown in Fig.13. The inverse of the slope of the linear fit to this set of data points is the

characteristic temperature T_0 value. T_0 value of 181 K is obtained at temperature range from 280 to 320 K, while T_0 value drop to 29 K above 320 K due to heating effects and the sharp change in the threshold current density with temperature at this temperature value as is shown in Fig.13.

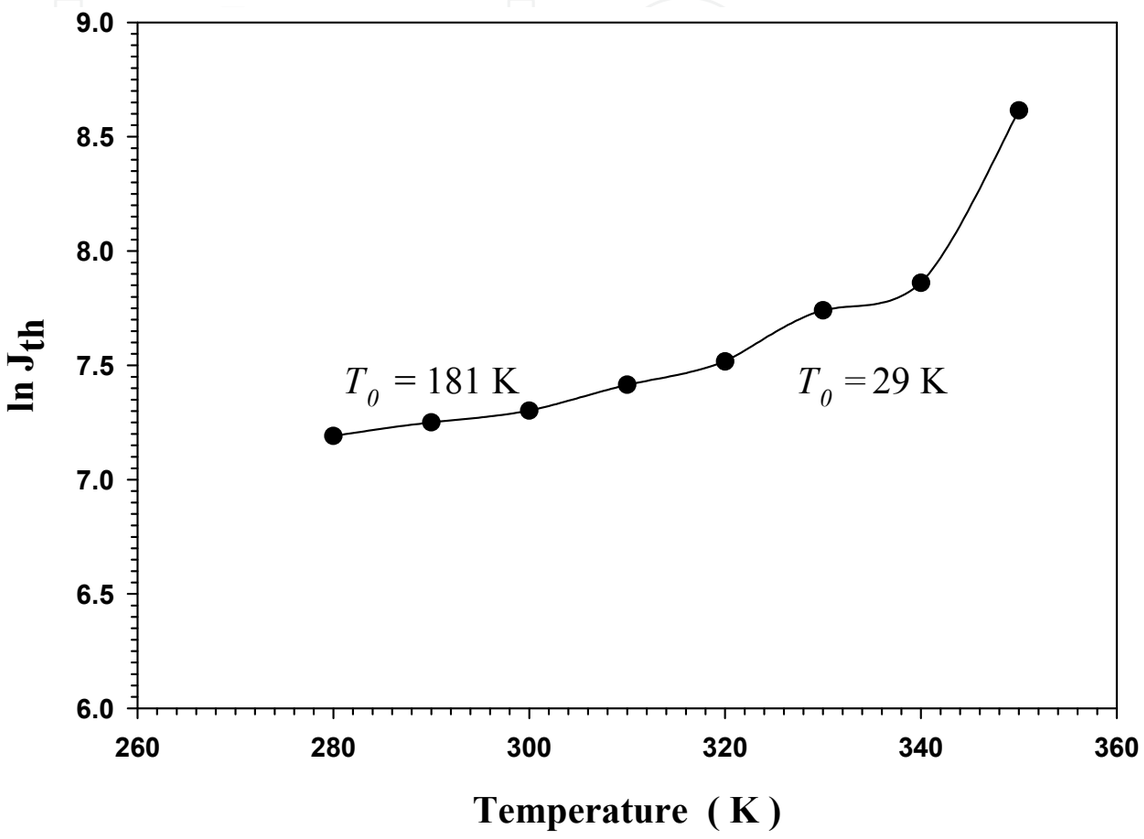


Fig. 13. The variations of the threshold current density (ln Jth) with increasing temperature of DQWs InGaN/ InGaN barrier LD.

6. InGaN/GaN multi quantum well laser diode

In this section the effect of changing the laser barrier layer in the active region from InGaN layer to GaN layer will be studied and investigated. The remaining laser diode layers are the same as in laser diode structure in section above. Figure 14 shows the output power, threshold current, slope efficiency, and external differential quantum efficiency (DQE) as a function of well numbers of InGaN/GaN laser diode. The simulation results indicate that the best laser performance is obtained when the number of QWs is two. For single quantum well (SQW), the gain begins to saturate before lasing is achieved while for triple quantum wells (TQWs), increase in current is needed to pump the additional wells above transparency. A maximum output power of 16.6 mW and lowest threshold current of 13.1

m A were obtained when the quantum well number was two. These results are in line with the other experimental results obtained by many researchers (Nakamura et al., 1998b; Nakamura et al., 2000).

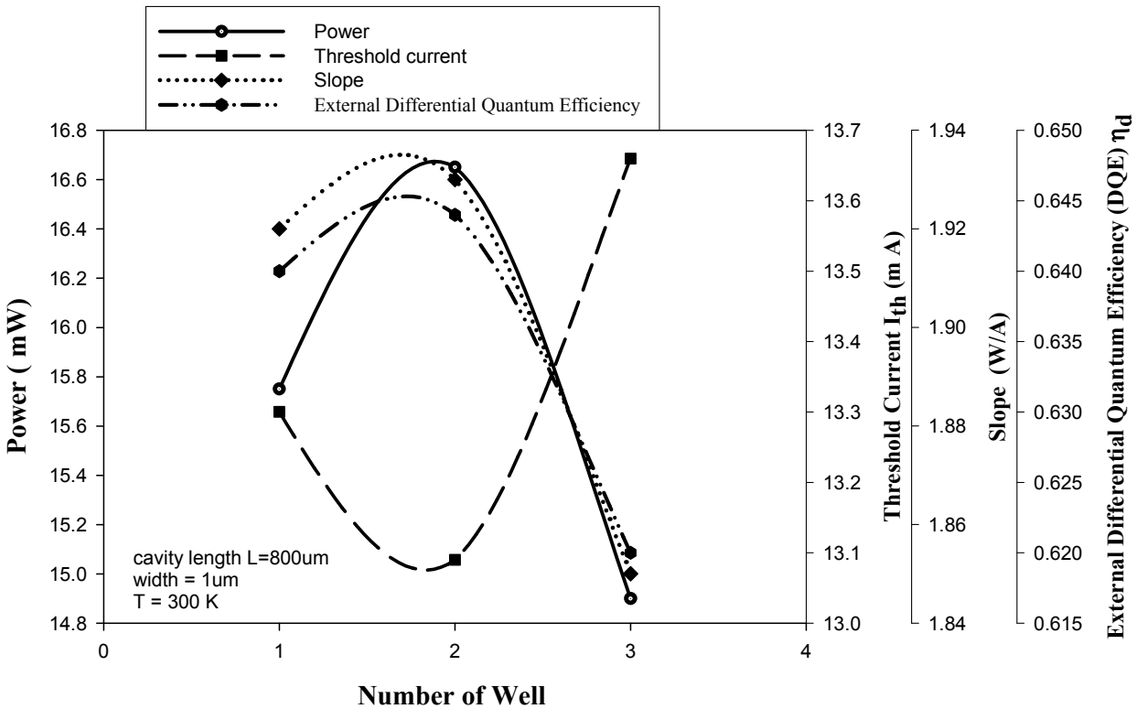


Fig. 14. The output power, threshold current density, slope efficiency and DQE as a function of quantum well number of InGaN/GaN LD.

6.1 Barrier doped and thickness effects on the performance of InGaN/InGaN laser diode

Figure 15 shows the effect of barrier doping on the output power and threshold current. We observed an increase in output power with increasing barrier doping concentration up to 30 m W for 1×10^{-19} cm^{-3} doing concentration. This may be attributed to the lowering of barrier heights in the active region with increased doping level. Low barrier heights lead to higher injection of carriers into the active region hence generating higher radiative recombinations at lower threshold currents. Also we investigated the effect of barrier thickness on the optical power and threshold current of InGaN MQWs laser. It was found that the $In_{0.01}Ga_{0.99}N$ barrier thickness also plays a key role in determining the optical characteristics of the InGaN MQWs laser diode.

Figure 16 shows that as the thickness of the $In_{0.01}Ga_{0.99}N$ barrier layer is increased, the output power decreases. Since the barrier width influences the strength of the internal fields in the wells and barriers, it also influences the absorption and gain. If the width of

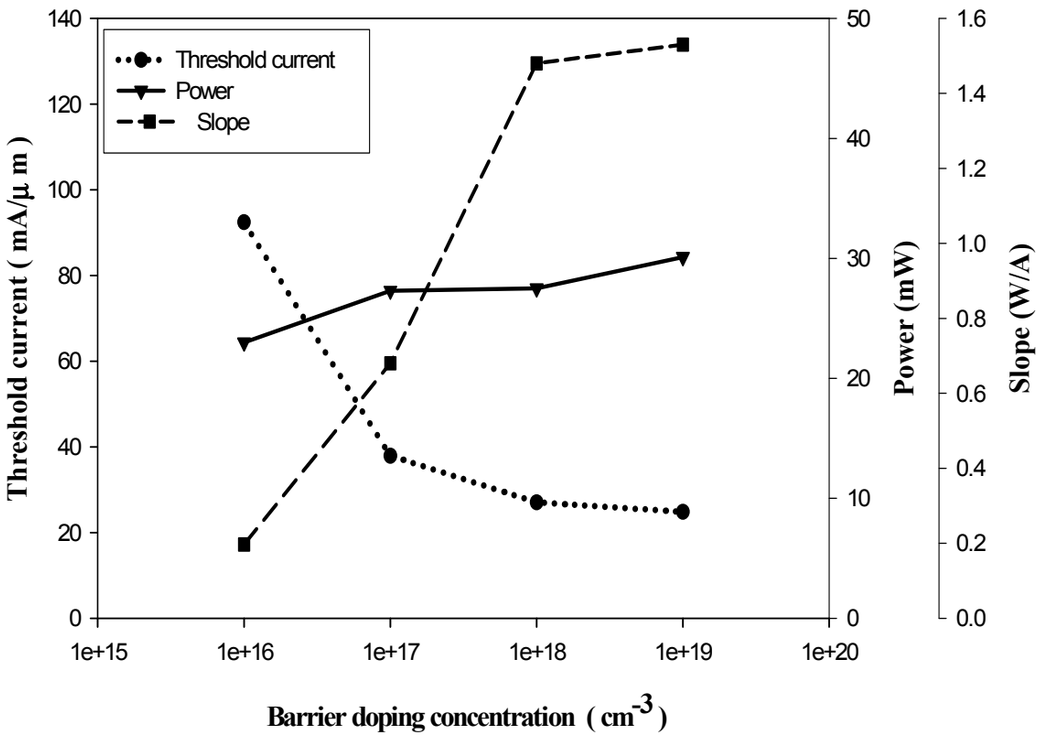


Fig. 15. Laser output power, slope efficiency, and threshold current as a function of barrier doping concentration.

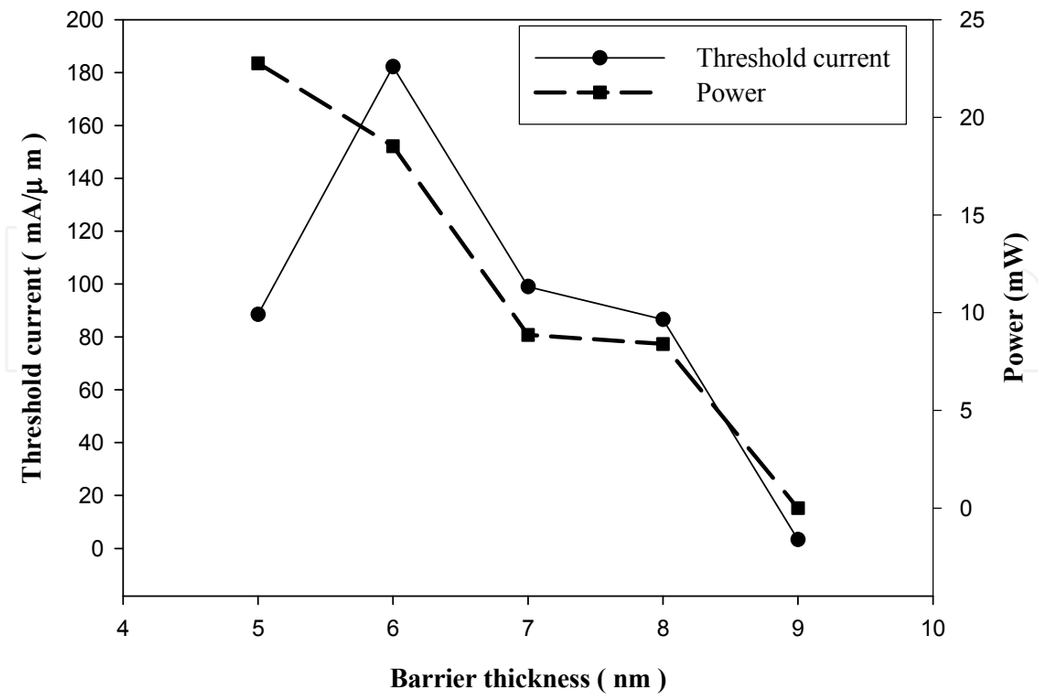


Fig. 16. Laser output power and threshold current as a function of barrier thickness.

the barriers is increased from 5nm to 9nm the internal field in the barriers is reduced. The most dominant result of this is that the electrons are no longer localized as closely to the well as before. The electrons are not confined in the well, but their confinement is provided by the tilted barriers. Thus, its localization is strongly influenced by the internal field in the barrier.

7. Summary

In this chapter we numerically investigated the performance of InGaN MQW with two different designs by changing the barrier layer type (InGaN and GaN). The effects of the well number, barrier thickness and doping on the laser performance were also studied and investigated. It was found that the problem of inhomogeneous carrier distribution in InGaN laser diode structures deteriorates with the increase of QW number for the spectral range under study. Thus, lowest threshold current is obtained when the number of InGaN well layers is two at our laser emission wavelength. We also observed that the barrier thickness and doping play important roles to determine the laser diode performance. Our simulation results in this study are in agreement with the experimental results observed by Nakamura et al. (1998a; 2000)

8. References

Domen, K., Soejima, R. Kuramata, A., Horino, K., Kubota, S., and Tanahashi, T.,(1998) "Interwell inhomogeneity of carrier injection in InGaN/GaN/AlGaN multiquantum well lasers" , *Appl. Phys. Lett*., Vol.73, No.19.

Fritsch, D., Schmidt, H. and Grundmann, M., (2003) "Band–structure pseudopotential calculation of zinc-blende and wurtzite AlN,GaN, and InN ", *Phys. Rev.B*, Vol. 67,p. 235

Jiang. H., Lin, J., (2001) "Advances in III-nitride micro-photonic devices", Proc. 14th Annual Meeting of the IEEE Lasers and Electro-Optics Society, 12-13 Nov. 2001, LEOS 2001, Vol. 2, pp.758 – 759.

Kuo, Y., Liou, B., Chen M., Yen, S., Lin, C., (2004), "Effect of band-offset ratio on analysis of violet–blue InGaN laser characteristics", *Optics Communications*, Vol. 231,pp.395–402.

Nakamura, S. and Fasol, G. (1997) in: "The Blue Laser Diode", Springer, and Heidelberg.

Nakamura, S., Senoh, M., Nagahama, S., Iwasa, N., Matsushita, T., and Mukai, T., (2000), "Blue InGaN-based laser diodes with an emission wavelength of 450 nm", *Appl. Phys. Lett*, Vol.76, p.22.

Nakamura, S., Senoh, M., Nagahama, S., Iwasa, N., Yamada, T., Matsushita, T., Kiyoku,H. Sugimoto,Y. Kozaki,T. Umemoto,H. Sano, M. and Chocho, K. (1998b) "InGaN/GaN/AlGaN-Based Laser Diodes Grown on GaN Substrates with a Fundamental Transverse Mode", Jpn.J. Appl. Phys., Vol.37, p.L1020.

Nakamura, S., Senoh,M., Nagahama, S., Iwasa,N., Yamada,T., Matsushita,T., Kiyoku,H., Sugimoto,Y., Kozaki,T., Umemoto,H., Sano, M., and Chocho,K., (1998a) "Violet InGaN/GaN/AlGaN-Based Laser Diodes with an Output Power of 420 mW", *Jpn..J.Appl.Phys*., Vol.37, p.L627.

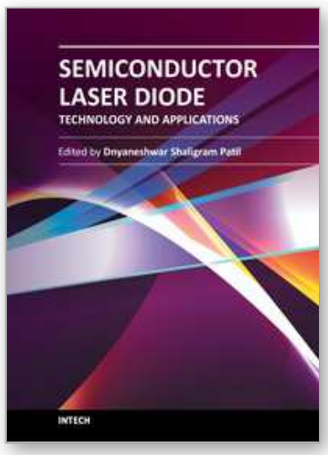
Ponce. F. A. and Bour. D. P., (1997) "Nitride-based semiconductors for blue and green light-emitting devices", *Nature*, Vol.386, p.351.

Sink, R.K., (2000) "Cleaved-Facet III- Nitride Laser Diode," Ph.D. Thesis, Electrical and Computer Engineering, University of California at Santa Barbara.

Stringfellow, G. B. and Craford, M. G., (1997) "High Brightness Light-emitting Diodes", *Semiconductors and Semimetals* Vol. 48, Academic, San Diego

IntechOpen

IntechOpen



Semiconductor Laser Diode Technology and Applications

Edited by Dr. Dnyaneshwar Shaligram Patil

ISBN 978-953-51-0549-7
Hard cover, 376 pages
Publisher InTech
Published online 25, April, 2012
Published in print edition April, 2012

This book represents a unique collection of the latest developments in the rapidly developing world of semiconductor laser diode technology and applications. An international group of distinguished contributors have covered particular aspects and the book includes optimization of semiconductor laser diode parameters for fascinating applications. This collection of chapters will be of considerable interest to engineers, scientists, technologists and physicists working in research and development in the field of semiconductor laser diode, as well as to young researchers who are at the beginning of their career.

How to reference

In order to correctly reference this scholarly work, feel free to copy and paste the following:

Sabah M. Thahab (2012). Characterization Parameters of (InGaN/InGaN) and (InGaN/GaN) Quantum Well Laser Diode, Semiconductor Laser Diode Technology and Applications, Dr. Dnyaneshwar Shaligram Patil (Ed.), ISBN: 978-953-51-0549-7, InTech, Available from: http://www.intechopen.com/books/semiconductor-laser-diode-technology-and-applications/characterization-parameters-of-ingan-ingan-and-ingan-gan-quantum-well-laser-diode

INTECH
open science | open minds

InTech Europe
University Campus STeP Ri
Slavka Krautzeka 83/A
51000 Rijeka, Croatia
Phone: +385 (51) 770 447
Fax: +385 (51) 686 166
www.intechopen.com

InTech China
Unit 405, Office Block, Hotel Equatorial Shanghai
No.65, Yan An Road (West), Shanghai, 200040, China
中国上海市延安西路65号上海国际贵都大饭店办公楼405单元
Phone: +86-21-62489820
Fax: +86-21-62489821

© 2012 The Author(s). Licensee IntechOpen. This is an open access article distributed under the terms of the Creative Commons Attribution 3.0 License, which permits unrestricted use, distribution, and reproduction in any medium, provided the original work is properly cited.

IntechOpen

IntechOpen